Supporting Information

Novel Polyethylene Fibers of Very High Thermal Conductivity Enabled by Amorphous Restructuring

*Bowen Zhu,[†] Jing Liu,[†] Tianyu Wang,[†] Meng Han,[†] Shah Valloppilly,[‡] Shen Xu,[§, *]*

*Xinwei Wang[†, *]*

[†]Department of Mechanical Engineering, Iowa State University, Ames, IA 50011, United States

[‡]Nebraska Center for Materials and Nanoscience, University of Nebraska-Lincoln, Lincoln, NE 68588, United States

[§]Automotive Engineering College, Shanghai University of Engineering Science, 333 Longteng Road, 201620 Shanghai, P. R. China

---

[*] Corresponding authors. Email: xwang3@iastate.edu (X.W.), shxu16@sues.edu.cn (S.X.).
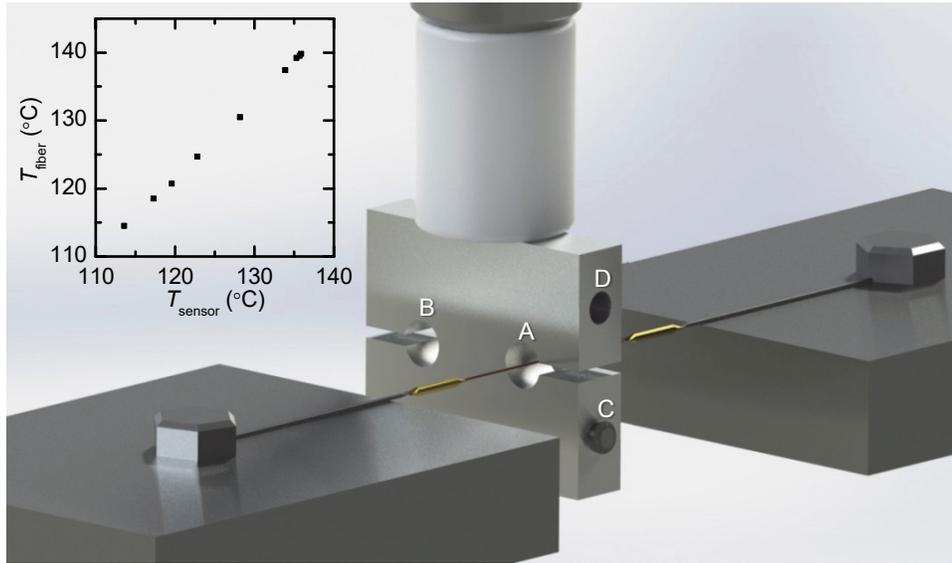
Heat Stretching

Figure S1. Experimental set-up for heat stretching. Hole A is the fiber hole with a slit. The slit is designed for inserting and removing the fiber. Hole B is a substitute for the hole A. Hole C and D are occupied with a cartridge heater and a thermocouple sensor respectively. The inset gives the relationship between the temperature of the heated fiber and that of the thermocouple sensor.

To stretch fiber samples at a controllable speed and temperature, a heat stretching system is designed based on the fiber tapering method introduced by Rudy and colleagues.[1] As presented in **Figure S1**, the speed control part is composed of two motorized translation stages (Thorlabs MTS50-Z8/Z812B), which move in opposite direction at the same speed during heat stretching. The motion of the stages is delivered to the fiber via fishing lines (UHMW-PE multiple filaments), with flattened brass tubes and screws as connection. The length of the suspended sample is ~ 35 mm, while the width of the Al block as heater is ~ 3 mm. The elongation of fishing line has been verified to be negligible compared with the elongation of stretched samples. We marked both ends of the sample with ink dots. The motion of the ink dots was found to be identical to that of the translation stages.

To monitor and control temperature, an aluminum (Al) block is machined to accommodate a sample fiber, a thermocouple and a cartridge heater as seen in **Figure S1**. The cartridge heater (in hole C) and thermal couple (in hole D) enable spontaneously monitoring and adjusting temperature. The temperature of the Al block is maintained stable ($\pm$ 1 ºC) during a single stretching run. When the Al block is heated to a desired temperature, the fiber is fed into the fiber hole through the narrow slit. Then the two translation stages move with a constant speed in opposite direction, until the sample reaches its expected maximum elongation (slightly smaller than the elongation at break for numerous samples). Once the stretching process is completed, the fiber is removed from the Al block and cooled down in ambient air (20 ºC). It should be mentioned that the temperature given by the thermocouple sensor (T_{sensor}) is correlated to but still differs a little from the temperature of the center of the heated region in sample (T_{fiber}). Therefore, a preliminary test was performed to evaluate the difference. A very thin sensor (25-µm-thick type T thermocouple, Omega 5TC-TT-T-36-36) was attached to the center of the heated region with a touch of silver paste. The temperature difference is shown in the inset of **Figure S1**. The additional sensor is not applied to the to-be-stretched samples. All the stretching temperatures mentioned in this work are T_{fiber}.

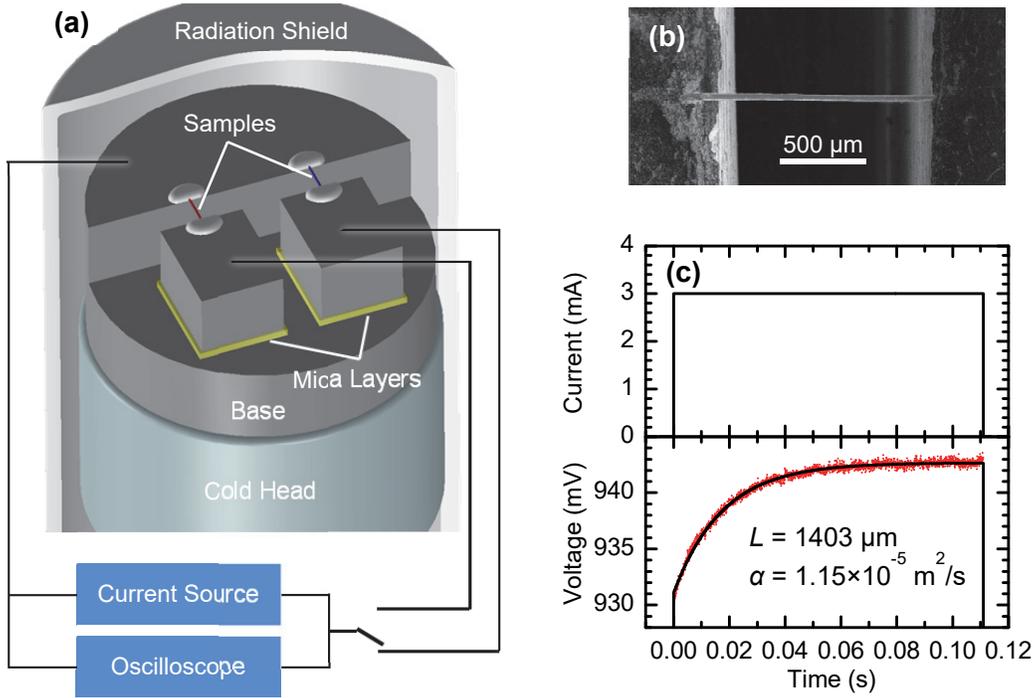**Transient Electro-thermal (TET) Technique**

Figure S2. (a) Experiment set-up for thermal characterization. In a vacuum chamber with radiation shield, the to-be-measured sample fibers are mounted on an Al base and two Al electrodes. The base and electrodes are further connected to a DC current source and an oscilloscope. Thin mica layers are employed to electrically isolate the electrodes from the base. The Al base is attached to the cold head of a cryogenic system (JANIS CCS-450) by thermal grease. **(b)** SEM image of a sample prepared for TET characterization. **(c)** TET data for the sample measured at room temperature. The data include square current input, voltage output obtained by oscilloscope and, fitted voltage-time curve. The thermal diffusivity is obtained through the fitting, with given sample length.

The TET technique integrated with a cryogenic system allows measurements of thermal diffusivity α in the temperature range from RT to 30 K. The experimental set-up is presented in **Figure S2** (a). A stretched fiber and its reference sample (red fiber and blue fiber) are connected to an Al base and two Al electrodes. Silver paste is employed to guarantee a sound electrical and thermal contact between Al electrode and sample fiber. The two electrodes are electrically insulated from the Al base by thin mica layers. The electrodes and samples are placed in cryostat

(CCS-450, JANIS). The Al base shared by both fibers is attached to the cold head with thermal grease in between. High vacuum (0.4 ~ 0.6 mTorr) and radiation shield are used to reduce the effect of heat convection and radiation. A current source (Keithley 6221) and an oscilloscope (Tektronix DPO3052) are connected to the Al base and electrodes to feed current and monitor the voltage evolution over the fibers. **Figure S2**(b) presents the SEM image of an original UHMWPE fiber, named as sample C in the following discussion, mounted on electrodes. The fiber is suspended over a 1.3 mm gap between Al base and electrode. The thickness of fibers before and after stretching is in the range of 15 ~ 50 μm.

The general idea of TET is to translate transient temperature change induced by electrical heating into electrical signals. A 20-nm thick Ir layer (Quorym Q150T S) is coated on the sample fiber as heater and temperature sensor. During measurement, a step current (1 ~ 5 mA) is fed through the Ir coating to induce Joule heating. As a result of heat dissipation and constant heating (in a single step), the average temperature of the fiber gradually increases by ~ 15 K and hence reaches steady state. The temperature rise leads to an increase of electrical resistance for Ir, which has a positive temperature coefficient of resistance (TCR). The resistance increase finally appears as voltage evolution monitored by oscilloscope. Like the evolution of the average temperature, the voltage rises up with a decreasing speed until reaches a plateau, indicating the steady state of heat dissipation. Therefore, the voltage evolution history is tightly related to α. **Figure S2** (c) presents the current input (a single square wave) and voltage change in response. There are approximately 1000 ~ 2000 data points for a single voltage peak. Note that the coating is thin enough (20 nm) so that the coating's temperature yields to the sample's temperature. The heat conduction along the sample can be simplified as a one-dimensional transient heat transfer

model. The temperature of the electrodes is assumed unchanged during the Joule heating owing to the much larger volume of the electrode than that of the sample fiber. By solving the governing equation of the model (q is Joule heating term),

$$\frac{\partial(\rho c_p T)}{\partial t} = k\frac{\partial^2 T}{\partial x^2} + q \tag{1}$$

the normalized temperature can be expressed as: [2]

$$T^* = \frac{96}{\pi}\sum_{m=1}^{\infty}\frac{1-\exp[-(2m-1)^2\pi^2\alpha_{eff}t/L^2]}{(2m-1)^4} \tag{2}$$

where α_{eff} is the sample's effective α including the contribution from thermal radiation and Ir coating. In calculation, the first 2000 terms of the infinite series are summed up to approximate the infinite sum. Here, TCR can be considered as constant since the current-induced temperature rise is not large, ~17 °C for the sampled UHMW-PE fibers. The constant TCR allows the normalized voltage evolution to mimic the normalized temperature rise in the form of $T^* = (V - V_0)/(V_1 - V_0)$. V_0 and V_1 are the initial voltage and steady-state voltage, respectively. Therefore, temperature change is translated into voltage evolution. By fitting the transient voltage curve with non-linear least square method, α_{eff} can be obtained. The real thermal diffusivity α_{real} is acquired by subtract the radiation term and coating term using the following formula[2]

$$\alpha_{real} = \alpha_{eff} - \frac{16\varepsilon\sigma T^3 L^2}{\pi^2 D\rho c_p} - \frac{L_{Lorenz}TL}{RA\rho c_p} \tag{3}$$

where σ is Stefan-Boltzmann constant, L_{Lorenz} and R are the Lorenz number and electrical resistance of the Ir coating, ε, ρc_p, D and A are the emissivity, diameter, volumetric heat capacity, and cross-sectional area of the fiber sample, respectively. The radiation effect and Ir coating effect are found negligible. Both of them are two orders of magnitude smaller than α_{eff}. For example, for a 1700-μm long original UHMWPE fiber, the radiation effect and coating effect are

calculated to be 1.2×10^{-7} m^2/s and 3.8×10^{-8} m^2/s while the measured α_{eff} is 2.4×10^{-5} m^2/s at RT. Hence α_{eff} is simply denoted as α. For a more complete description of physical principle and experimental design about the TET technique, readers are referred to our previous publications.[2-5]

k is calculated by $k = \alpha \rho c_p$, where ρc_p is volumetric heat capacity. ρc_p of original UHMW-PE fiber has been studied in Liu's work by using TET and molecular dynamic simulation together. (Note that TET characterization of ρc_p has larger error than that of α. Numerical simulation is utilized to help error correction.).[2, 6] Here we can assume that ρc_p of stretched samples is identical to that of un-stretched ones for two reasons: 1) for amorphous PE and crystal PE the difference in ρc_p is not significant (within 20% in the temperature range of 30 ~ 300 K), and 2) the stretching-induced crystallinity reduction (from 92% to 83%) is not overwhelmingly large.[7]

The strain ratio is determined by the effective cross-sectional area in thermal conduction rather than the measured thickness in SEM images, due to S-900's irregular shape of cross section. The approach is shown as follows. The steady-state solution in TET includes both k and cross-section area A_c, while k has been solved using is $k = \alpha \rho c_p$. α has been solved in the transient expression. ρc_p is referred to literature. Therefore, A_c can be calculated using steady-state solution: $A_c = I^2 R L / 12 k \Delta T$. In the equation, I is amplitude of the step current, ΔT is the resultant temperature rise, R is the electrical resistance of the Ir coating at steady state, and L is the fiber length. ΔT is gauged from electrical resistance ΔR with R-T correlation recorded in the cryogenic experiment.

Thermal Reffusivity and Defect-induced Phonon Mean Free Path

The defect-induced phonon MFP can be evaluated by Θ, reciprocal of α, at the 0 K limit. Under relaxation time approximation, Θ can be expressed as $\Theta = 3v^{-1}l^{-1}$, where v is the phonon group velocity and l is the phonon MFP. l consists of two contributions: $l^{-1} = l_0^{-1} + l_i^{-1}$, where l_0 and l_i are induced by defect and phonon-phonon scattering, respectively. At low temperatures, the phonon-phonon scattering freezes out due to significantly reduced phonon population. Thus the expression of Θ reduces to $\Theta_0 = \Theta|_{T\to 0} = 3v^{-1}l_0^{-1}$. The relaxation time approximation is only intended for basic physics explanation. For a more accurate description about Θ_0 - l_0 correlation, all phonon dispersion and various phonon branches are considered based on the adaptive intermolecular reactive bond order (AIREBO) potential.[6] As $T\to 0$ K, phonons with different frequencies are considered to share the same l_0 since only low-frequency/momentum acoustic phonons are excited according to Bose-Einstein distribution. Based on our earlier physics study of Θ_0 (the residual thermal reffusivity at the 0 K limit) of UHMWPE fibers,[3] we have

$$\Theta_0 = \frac{1}{\alpha}\bigg|_{T\to 0} = \frac{\rho c_p}{k}\bigg|_{T\to 0} = \frac{\rho c_p}{\rho c_p v l_0}\bigg|_{T\to 0} = \frac{\sum_{M=1}^{18}\int_0^{\omega_D} \partial U_M / \partial T d\omega}{\sum_{M=1}^{18}\int_0^{\omega_D} \partial U_M / \partial T l_0 v_\omega d\omega}\Bigg|_{T\to 0} \tag{4}$$

In the AIREBO model, PE crystals have 4 acoustic phonon branches and 14 optical phonon branches.[4] M denotes the number of phonon branches. U_M is the thermal energy for Mth phonon branch, v_ω is the phonon velocity dependent on frequency ω. ω_D is the cutoff frequency for each phonon branch. For acoustic phonon branches, the thermal energy U_M is given as:

$$U_M = \int g(\omega)n(\omega)\hbar\omega d\omega = \int_0^{\omega_D} g(\omega)\left(\frac{\hbar\omega}{e^{\hbar\omega/k_B T} - 1}\right)d\omega \tag{5}$$

where $g(\omega)$ is the density of state. The volumetric heat capacity C_a for the acoustic phonons is

$$C_a = \sum_{M=1}^{4} \int_0^{\omega_D} g(\omega) k_B \left(\frac{\hbar\omega}{k_B T} \right)^2 \frac{e^{\hbar\omega/k_B T}}{(e^{\hbar\omega/k_B T} - 1)^2} d\omega \tag{6}$$

For optical phonons, the thermal energy is given by the Einstein model：$U = N < n > \hbar\omega$, among which N is the number of primitive cells. Thus we have

$$C_o = \sum_{M=1}^{14} N k_B \left(\frac{\hbar\omega}{k_B T} \right)^2 \frac{e^{\hbar\omega/k_B T}}{(e^{\hbar\omega/k_B T} - 1)^2} \tag{7}$$

The total volumetric heat capacity is the combination of two kinds of phonons. The accuracy of this heat capacity calculation is evaluated by comparing with experimental results.[5] Sound agreement has been observed and discussed in detail in our past work. Optical phonon branches contribute much less to the heat capacity compared with acoustic phonon branches. With the physics that the optical phonons have almost zero phonon velocity and significantly smaller heat capacity, acoustic phonons are the major heat carriers in the thermal transport in polymers. Therefore only acoustic phonons are considered for the estimation of the phonon velocities. The phonon velocity is $v_\omega = \partial\omega(\kappa)/\partial\kappa$. The phonon velocity will be used in evaluating the MFP due to defect (l_0). Combining Eqs. (3)-(6), Θ_0 is obtained as:

$$\Theta_0 = \left. \frac{\sum_{M=1}^{4} \int_0^{\omega_D} g(\omega) k_B (\hbar\omega/k_B T)^2 e^{\hbar\omega/k_B T} / (e^{\hbar\omega/k_B T} - 1)^2 d\omega + \sum_{M=5}^{18} k_B (\hbar\omega/k_B T)^2 e^{\hbar\omega/k_B T} / (e^{\hbar\omega/k_B T} - 1)^2}{l_0 \sum_{M=1}^{4} \int_0^{\omega_D} g(\omega) k_B (\hbar\omega/k_B T)^2 e^{\hbar\omega/k_B T} / (e^{\hbar\omega/k_B T} - 1)^2 v_\omega d\omega} \right|_{T \to 0}$$

$$\tag{8}$$

With Eq. (7), we are able to determine l_0 by knowing Θ_0, $g(\omega)$, and v_ω. The dependence of $g(\omega)$ and v_ω on ω has been given and discussed in our previous work.[3]

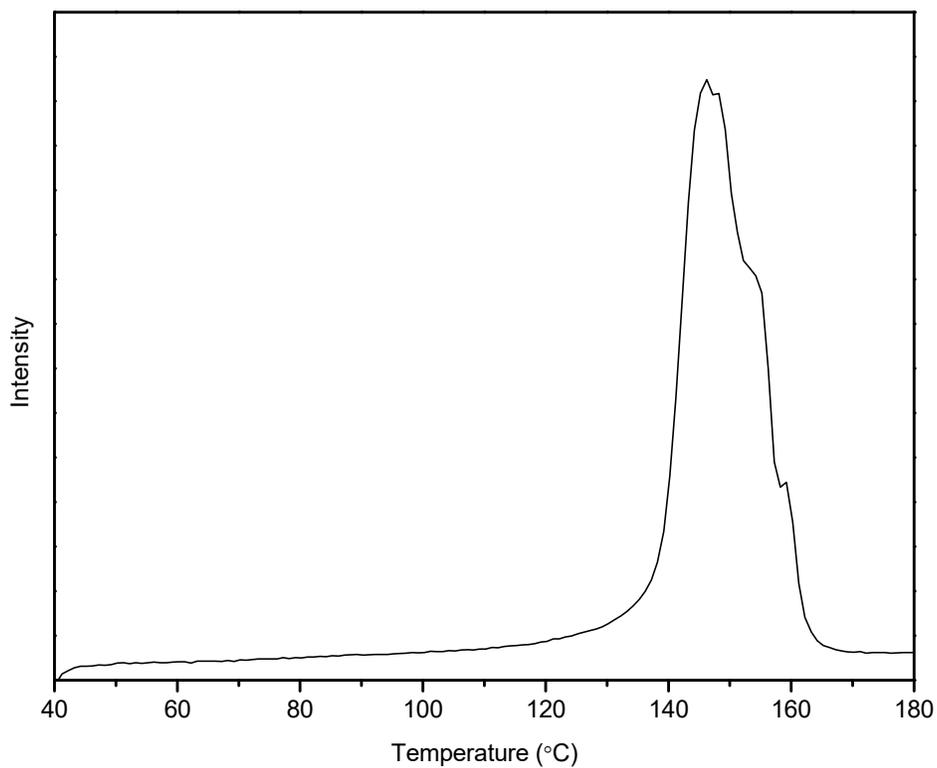**Differential Scanning Calorimeter of Original S-900 fiber**

Figure S3 Differential scanning calorimeter analysis for original Spectra S-900 fiber. The scanning rate is 5 K/min. The scanning range is from 40 to 180 $^{\circ}$C. Sample weight is 3.4078 mg.

REFERENCES

1.   Rudy, C. W.; Marandi, A.; Vodopyanov, K. L.; Byer, R. L., In-situ Tapering of Chalcogenide Fiber for Mid-infrared Supercontinuum Generation. **2013,** (75), e50518.

2.   Liu, J.; Xu, Z.; Cheng, Z.; Xu, S.; Wang, X., Thermal Conductivity of Ultrahigh Molecular Weight Polyethylene Crystal: Defect Effect Uncovered by 0 K Limit Phonon Diffusion. *ACS Applied Materials & Interfaces* **2015,** *7* (49), 27279-27288.

3.   Guo, J.; Wang, X.; Wang, T., Thermal characterization of microscale conductive and nonconductive wires using transient electrothermal technique. *Journal of Applied Physics* **2007,** *101* (6), 063537.

4.   Xu, Z.; Wang, X.; Xie, H., Promoted electron transport and sustained phonon transport by DNA down to 10 K. *Polymer* **2014,** *55* (24), 6373-6380.

5.   Lin, H.; Xu, S.; Wang, X.; Mei, N., Thermal and Electrical Conduction in Ultrathin Metallic Films: 7 nm down to Sub-Nanometer Thickness. *Small* **2013,** *9* (15), 2585-2594.

6.   Henry, A.; Chen, G., High thermal conductivity of single polyethylene chains using molecular dynamics simulations. *Physical review letters* **2008,** *101* (23), 235502.

7.   Chang, S., Heat-capacities of polyethylene from 2 to 360 K. 2. 2 High-density linear polyethylene samples and thermodynamic properties of crystalline linear polyethylene. *Journal of Research of the National Bureau of Standards Section A-Physics and Chemistry* **1974,** (3), 387-400.